Applied Catalysis B: Environmental 119–120 (2012) 49–55

Contents lists available at SciVerse ScienceDirect

Applied Catalysis B: Environmental

journal homepage: www.elsevier.com/locate/apcatb

In-situ plasma regeneration of deactivated Au/TiO_2 nanocatalysts during CO oxidation and effect of N_2 content

Hong-Yu Fan, Chuan Shi, Xiao-Song Li, Shuo Zhang, Jing-Lin Liu, Ai-Min Zhu*

Laboratory of Plasma Physical Chemistry, School of Physics and Optoelectronic Engineering & School of Chemistry, Dalian University of Technology, Dalian 116024, China

ARTICLE INFO

Article history:
Received 17 November 2011
Received in revised form 14 February 2012
Accepted 16 February 2012
Available online 24 February 2012

Keywords:
Gold catalyst
Deactivation
Plasma regeneration
N_2 content
CO oxidation

ABSTRACT

Driven by excellent CO oxidation capability of gold nanocatalysts at room temperature, a TiO_2 supported Au nanocatalyst (Au/TiO_2) was synthesized by deposition–precipitation method. To solve the deactivation issue of Au/TiO_2 catalyst during CO oxidation, in-situ regeneration by N_2/O_2 plasma was employed. Pure O_2 plasma could reversibly regenerate the deactivated Au/TiO_2 catalyst, however, N_2 addition resulted in an extra catalyst poisoning during regeneration. The extra poisoning effect was the most severe at 10% N_2 and became much weaker at 80% N_2. To investigate the formation of any surface poisoning species $[NO_y]_s$ on Au/TiO_2 catalyst, gaseous product of N_2/O_2 plasma over fresh Au/TiO_2 catalyst was on-line analyzed by FT-IR, followed by catalyst characterization with temperature programmed desorption (TPD), X-ray photoelectron spectroscopy (XPS), UV–vis spectroscopy and diffuse reflectance infrared Fourier transform (DRIFT) spectroscopy. The Au/TiO_2 catalysts before and after plasma regeneration were also measured by transmission electron microscopy (TEM), in order to exclude the poisoning effect arisen from the change in gold particle size or morphology.

1. Introduction

Supported gold (Au) nanocatalyst attracts much attention due to its exceptionally high activity on CO oxidation at low-temperature [1]. Catalysis of gold nanoparticle for CO oxidation could be widely applied in environmental protection, clean energy conversion, and various industrial processes and instrument fields, such as indoor air purification, polymer electrolyte membrane (PEM) fuel cells, closed CO_2 laser, low-temperature CO sensors, and gas mask [2–5]. However, deactivation of gold catalyst during storage and reaction [6,7] is a major issue preventing it from many practical applications. In general, two major reasons for gold catalyst deactivation during CO oxidation reaction were put forward and accepted, i.e. agglomeration of gold particles and accumulation of carbonate-like species. The agglomeration of gold particles causes an irreversible and weak deactivation [8–12], while the accumulation of inactive surface carbonate species on catalyst during CO oxidation leads to a reversible deactivation [13–19]. The latter deactivation could be reversibly regenerated via heat-treatment, with a side effect of irreversible gold particles aggregation.

Non-thermal plasma (NTP) technologies [20], such as sub-atmospheric-pressure plasma with ionic liquid [21] and atmospheric-pressure helium plasma [22,23], were employed to prepare or activate gold catalysts at room temperature. Oxygen plasma or ozone injection was reported to be effective for regeneration of deactivated gold catalysts caused by toluene and propylene adsorption [24]. To the best of our knowledge, there has been no report on plasma regeneration of deactivated gold catalyst during CO oxidation.

In this paper, O_2 plasma was explored to in-situ regenerate deactivated Au/TiO_2 catalyst during CO oxidation at low temperature. From practical point of view, it is more favorable to use air instead of pure O_2 for the regeneration. Therefore, the effect of N_2 addition to oxygen was also investigated on the effectiveness of plasma regeneration. Combined with FT-IR analysis of the gaseous product, deactivated catalyst was characterized by temperature programmed desorption (TPD), UV–visible spectroscopy (UV–vis) and diffuse reflectance infrared Fourier transform spectroscopy (DRIFTs). Moreover, the formation of surface poisoning species $[NO_y]_s$ during N_2/O_2 plasma regeneration was proposed to illustrate the mechanism of catalyst poisoning.

2. Experimental

2.1. Reactor and catalyst activity evaluation

A dielectric barrier discharge (DBD) reactor was used to generate plasma at atmospheric pressure. It consisted of a quartz tube (inner diameter of 8.5 mm, wall thickness of 1 mm), a stainless steel rod (diameter of 3 mm) inserted along the axial direction of

* Corresponding author. Tel.: +86 411 84706094; fax: +86 411 84706094.
E-mail address: amzhu@dlut.edu.cn (A.-M. Zhu).

0926-3373/$ – see front matter © 2012 Elsevier B.V. All rights reserved.
doi:10.1016/j.apcatb.2012.02.016

the quartz tube as a high-voltage electrode, and catalyst pellets (500 mg, 20–40 mesh) located between the quartz tube and the central electrode rod. A stainless steel wire mesh was wound on the outside surface of the quartz tube as a grounded electrode. High voltage with an AC frequency of 2 kHz and input power of 18 W were applied. To regenerate deactivated (or to treat fresh) gold catalysts by plasma, 200 mL/min of O_2, N_2 or N_2/O_2 (N_2 content ranging from 5% to 80% by volume) was flowed through the DBD reactor during 20-min discharge time. The gaseous products from plasma regeneration or treatment were on-line monitored using an FT-IR (IGS, Thermofisher, USA) equipped with a gas cell (2 m in optical path length).

The activity of Au/TiO_2 catalyst was measured at room temperature in the above-mentioned reactor (plasma off). The reactor was packed with 100, 250 or 500 mg of catalyst at a gas hourly space velocity (GHSV) of 300,000, 120,000 or 60,000 h^{-1}, respectively. A gaseous mixture stream (simulated air, 80% N_2/20% O_2) containing 960–970 ppm of CO was fed into the reactor at 600 mL/min and 50% relative humidity (RH, 298 K). The outlet concentration CO and CO_2 was on-line analyzed by an infrared absorption spectrometer (SICK-MAIHAK-S710, Germany). CO conversion was defined in the following equation:

$$\text{CO conversion} = \frac{C_{CO_2}^{out}}{C_{CO}^{in}} \times 100\%$$

where, C_{CO}^{in} is the volume concentration of CO at reactor inlet and $C_{CO_2}^{out}$ is the volume concentration of CO_2 at reactor outlet.

2.2. Catalyst preparation and characterization

The Au/TiO_2 catalyst with nominal gold loading at 1 wt.% was prepared by deposition–precipitation method. $HAuCl_4$ (11 mL, 10 g/L) solution was first mixed with 5.0 g of TiO_2 (Degussa P25) and then diluted with 200 mL of deionized (D.I.) water. Subsequently, a designated amount of urea with a molar ratio of gold to urea at 1/200 was added as the precipitation agent. The mixture was stirred at 353 K for 8 h and aged for 12 h at room temperature, followed by filtration to separate the precipitate from the solution. The filtered cake was washed three times with D.I. water, dried in air at 353 K for 6 h, and calcined in air at 573 K for 2 h.

The final gold loading in Au/TiO_2 catalyst was about 0.6 wt.%, as determined by inductively coupled plasma-atomic emission spectroscopy (ICP-AES, Optima 2000DV, USA). The catalyst particle size and morphology before and after plasma treatment were observed by transmission electron microscopy (TEM) (Tecnai G^2 spirit, Hong Kong). The surface species on the catalyst after N_2/O_2 plasma treatment was studied by temperature programmed desorption, UV–visible spectroscopy (UV-550, Japan) and diffuse reflectance infrared Fourier transform spectroscopy (Bruker Tensor 27, Germany). TPD experiments were performed in helium (99.999%) at a flow rate of 200 mL/min, a ramping rate at 10 K/min from 303 to 573 K, and a 1-h hold at 573 K. The outlet gas was monitored on-line using a mass spectrometer (MS, Hiden HPR20, UK). The surface chemical states of Au/TiO_2 catalysts were examined by a X-ray photoelectron spectroscopy (XPS, Kratos Axis Ultra DLD, UK) with a mono Al Kα X-ray source, operated at 40 eV for high resolution spectra. The reference energy used for calibration was the C 1s signal at 284.6 eV.

3. Results and discussion

3.1. Catalyst deactivation and reversible regeneration by O_2 plasma

Fig. 1 shows the variation in CO conversion on Au/TiO_2 catalyst at various GHSVs with time on stream (TOS). Obviously, the increase in GHSV resulted in not only a decrease in CO conversion but also an accelerated catalyst deactivation, which was reflected by the slope of the curves. For instance, the CO conversion of Au/TiO_2 catalyst at GHSV = 60,000 h^{-1} initially reached around 100%, then gradually dropped to 90% after 200-min TOS, due to the formation and accumulation of carbonates species on the gold catalyst surface [8]. In contrast, at higher GHSV (300,000 h^{-1}), the CO conversion rapidly dropped from 75% to 40% after 200-min TOS. Consequently, the deactivation phenomenon of Au/TiO_2 catalyst did exist in CO oxidation, which would require catalyst regeneration, in particular, reversible regeneration.

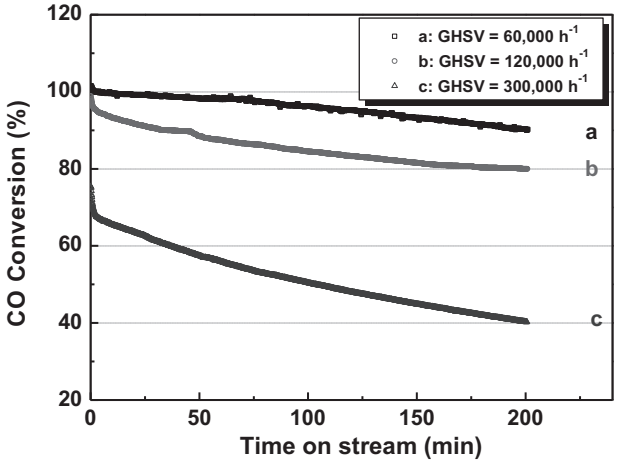

Fig. 1. CO conversion on Au/TiO_2 catalyst with time on stream at various gas hourly space velocities (GHSV): (a) 60,000 h^{-1}; (b) 120,000 h^{-1}; and (c) 300,000 h^{-1}.

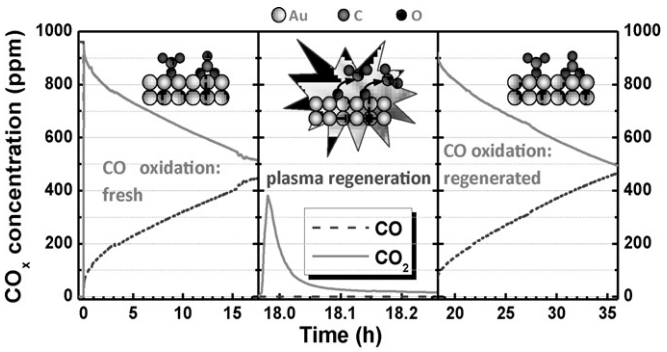

Fig. 2. Outlet concentration of CO and CO_2 with time on stream at different stages of operation: (a) CO oxidation on fresh Au/TiO_2 catalyst at 120,000 h^{-1} of GHSV; (b) regeneration of catalyst by O_2 plasma at a flow rate of 200 mL/min; and (c) CO oxidation on the regenerated catalysts at the same condition as in (a).

A series of experiments were designed to investigate reversible regeneration performance of oxygen plasma on the deactivated Au/TiO_2 catalyst. CO oxidation was first conducted on fresh Au/TiO_2 catalyst, the deactivated catalyst was then regenerated by O_2 plasma, and the regenerated catalyst was tested again with CO oxidation. Fig. 2 shows the outlet concentration of CO and CO_2 with time on stream at different stages of operation. In Fig. 2a, CO oxidation was performed on fresh Au/TiO_2 catalyst at 120,000 h^{-1} of GHSV. Significant deactivation of Au/TiO_2 catalyst occurred and CO conversion decreased from 98% to 53% over 17.6 h on stream. Subsequently, the deactivated catalyst was regenerated by O_2 plasma at 200 mL/min for 20 min. As shown in Fig. 2b, carbonates species on Au/TiO_2 catalyst were quickly converted into CO_2 within 2 min by O_2 plasma. In the next 3 min, very little CO_2 evolution was detected, indicating that most of surface carbonates species on Au/TiO_2 catalysts were removed by O_2 plasma. After 20-min O_2

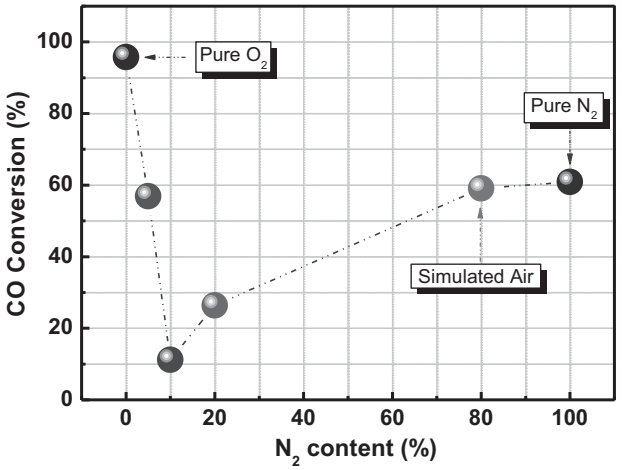

Fig. 3. CO conversion (GHSV = 60,000 h^{-1} and TOS = 30 min) on Au/TiO_2 catalyst regenerated by plasma with various N_2 content. The deactivated catalyst was obtained under the condition given in Fig. 1a.

plasma regeneration, CO oxidation was performed on the regenerated catalyst again. It can be clearly seen that the catalyst activity was fully restored, as indicated by the identical CO and CO_2 concentration profiles in Fig. 2a and c. As a blank experiment, the deactivated catalyst was purged with 200 mL/min of N_2 stream for 20 min (without plasma), but its catalytic activity was barely regenerated (not shown in Fig. 2). Consequently, the results clearly demonstrated that in-situ reversible regeneration of the deactivated Au/TiO_2 catalyst for CO oxidation could be successfully achieved by O_2 plasma, a fast and effective approach.

3.2. Effect of N_2 content on plasma regeneration

As driven by above-mentioned (Section 3.1) reversible regeneration of Au/TiO_2 catalyst by pure O_2 plasma and from a practical point of view, it is worth using air instead of pure O_2 for plasma regeneration. Fig. 3 shows CO conversion on the regenerated Au/TiO_2 catalyst by N_2/O_2 plasma at various N_2 contents. The deactivated catalyst was obtained from the fresh Au/TiO_2 catalyst undergoing CO oxidation at GHSV = 60,000 h^{-1} for 200 min, with CO conversion decreasing from 100% to 90%. Subsequently, the deactivated Au/TiO_2 catalyst was regenerated by N_2/O_2 plasma with 0–100% of N_2. Surprisingly, the activity of the regenerated catalyst was strongly dependent on N_2 content. CO conversion of the deactivated Au/TiO_2 catalyst could be recovered by pure O_2 plasma to 96% after 30 min on stream. On the contrary, N_2/O_2 plasma did not reversibly regenerate the Au/TiO_2 catalyst, and it even led to an extra poisoning effect. CO conversion dramatically dropped to 57%, reached the lowest level at 11%, and rose to 59% and 61% at N_2 contents of 5%, 10%, 80% and 100%, respectively. This extra poisoning effect of N_2/O_2 plasma on catalyst regeneration will be discussed in Section 3.3 in details. Encouragingly, at 80% N_2 (simulated air), the extra poisoning effect became much weaker, which is expected to be further minimized or completely removed via optimization of operation conditions in the future.

3.3. Mechanism of catalyst poisoning in N_2/O_2 plasma

3.3.1. Analysis of gaseous product from N_2/O_2 plasma

In order to clearly identify poisoning species and analyze gaseous product, all the starting catalyst samples used in Section 3.3 were fresh Au/TiO_2 catalysts. The gaseous product from N_2/O_2 plasma was analyzed on-line by FT-IR. Fig. 4 shows the FT-IR spectra of the gas product from N_2/O_2 plasma with various N_2 contents

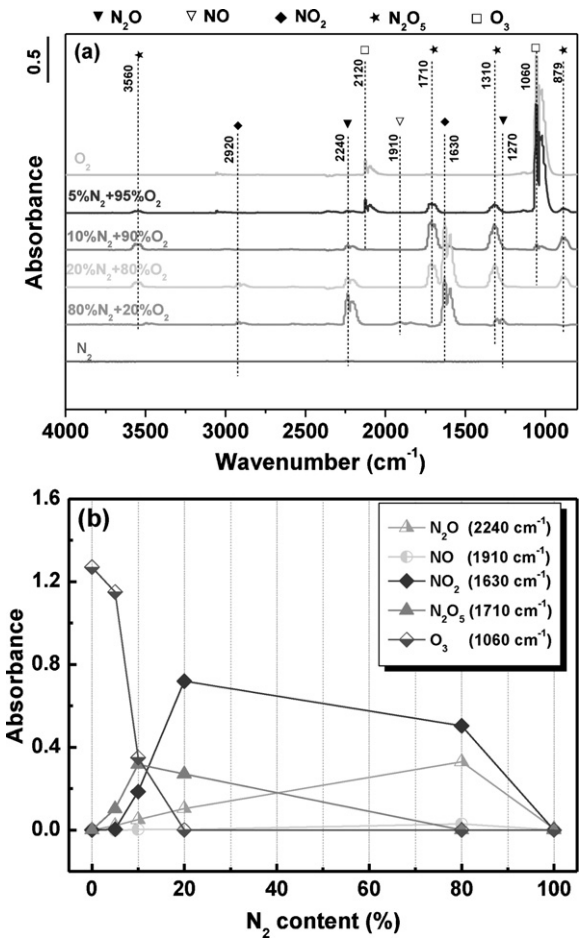

Fig. 4. (a) FT-IR spectra of the gaseous products from N_2/O_2 plasma with various N_2 contents; and (b) the IR peak intensity (absorbance) of formed O_3, N_2O_5, NO_2, N_2O and NO as a function of N_2 content. Data were obtained at 20-min discharge time.

and the plots of IR peak intensity of the formed O_3, N_2O_5, NO_2, N_2O and NO as a function of N_2 content. As shown in Fig. 4a, only O_3 with characteristic IR bands at 1060 and 2120 cm^{-1} was detected in pure O_2 plasma. At 5% N_2, some nitrogen oxides besides O_3 such as N_2O (2240 cm^{-1}, 2920 cm^{-1}) and N_2O_5 (879 cm^{-1}, 1310 cm^{-1}, 1710 cm^{-1}, 3560 cm^{-1}) were identified. At 10% N_2, O_3, N_2O, NO_2 (1590 cm^{-1}, 1630 cm^{-1}) and N_2O_5 existed in the gaseous products. NO (1910 cm^{-1}) was detected at 80% N_2. As shown in Fig. 4b, the intensities of NO_2 and N_2O_5 initially increased and reached maximum at N_2 contents of 20% and 10%, respectively, and thereafter reduced with N_2 content. For N_2O, its intensity increased monotonically with N_2 content up to 80%. In contrast, the intensity of O_3 decreased rapidly with N_2 content and almost dismissed at 20% of N_2.

To further illustrate formation pathways of the gaseous product detected by FT-IR, Table 1 listed proposed reactions in N_2/O_2 plasma and corresponding rate constants. NO formation was mainly due to the reaction of N atom with O_2 (R1–R3) and the reaction of N_2 (A) with O atom (R4). However, a rapid oxidation of NO to NO_2 via R7 and R9 led to almost no NO detection at N_2 content below 80% (O_2 content above 20%). NO_2 can react with N atom via R10 to form N_2O. On the other hand, NO_2 can be oxidized further to N_2O_5 via R11–R13. Due to the consumption of O atom and O_3 via R11 and R12, O_3 concentration decreased with increasing N_2 content, resulting in maximum concentration of N_2O_5 at 10% N_2. It is consistent with the most severe poisoning effect occurring at 10% N_2, as shown in Fig. 3, which also indicates that N_2O_5 formation contributed to the catalyst poisoning in N_2/O_2 plasma.

Table 1
Possible reactions in N_2/O_2 plasma and corresponding rate constants.

No.	Reaction	k_{298} (cm^3 $molecule^{-1}$ s^{-1})	References
R1	$N + O_2 \rightarrow NO + O$	8.5e−17	[25]
R2	$N(^2D) + O_2 \rightarrow NO + O$	4.2e−12	[26]
R3	$N(^2P) + O_2 \rightarrow NO + O$	2.0e−12	[27]
R4	$O + N_2(A) \rightarrow NO + N$	<6e−13	[28]
R5	$O + O_2 + M \rightarrow O_3 + M$	3.1e−14	[29]
R6	$O + O_3 \rightarrow O_2 + O_2$	8.0e−15	[30]
R7	$O + NO \rightarrow NO_2$	3.0e−11	[31,32]
R8	$O + NO_2 \rightarrow NO + O_2$	9.7e-12	[31,32]
R9	$NO + O_3 + M \rightarrow NO_2 + O_2 + M$	3.8e−12	[33]
R10	$NO_2 + N \rightarrow N_2O + O$	1.2e−11	[25]
R11	$O_3 + NO_2 \rightarrow NO_3 + O_2$	3.5e−17	[30]
R12	$O + NO_2 + M \rightarrow NO_3 + M$	1.8e−12	[30]
R13	$NO_3 + NO_2 + M \rightarrow N_2O_5 + M$	1.5e−12	[29]
R14	$O + NO_3 \rightarrow NO_2 + O_2$	1.7e−11	[29]

The third-body concentration [M] is about 2.4×10^{19} molecule/cm^3 at 298 K and 1 bar [34].

To elucidate the individual effect of various nitrogen oxides (except for N_2O_5 due to its instability) formed in N_2/O_2 plasma, CO oxidation in the presence of N_2O, NO or NO_2 over fresh Au/TiO_2 catalyst was examined. As shown in Fig. 5, the curve of CO conversion with TOS upon adding N_2O (curve b) is almost identical to that without adding any nitrogen oxides (curve a). This means that N_2O has no poisoning effect on the activity of Au/TiO_2 catalyst. Upon NO addition (curve c), a little decline in catalyst activity was observed. For either NO_2 addition from gas stream (curve d) or from NO_2 pre-adsorbed on catalyst (curve e), catalyst deactivation was significantly accelerated. However, the deactivation extent of the Au/TiO_2 catalyst in the presence of N_2O (b), NO (c) and NO_2 (d and e) was still not as deep as the catalysts treated by N_2/O_2 plasma (f), which can be deduced that the poisoning effect was mainly attributed to N_2O_5 formed in N_2/O_2 plasma.

3.3.2. Formation of surface poisoning species

Fig. 6 shows the TPD profiles of Au/TiO_2 catalyst treated in 10% N_2/90% O_2 plasma (input power at 18 W, 20 min). The MS signals of the effluent gas at m/z = 32 (O_2), m/z = 30 (NO, NO_2), m/z = 46 (NO_2) and m/z = 44 (N_2O) were scanned and recorded. Among them, MS signal at m/z = 30 was ascribed to either direct ionization of NO or dissociative ionization of NO_2 and N_2O. From Fig. 6e, it can be seen that there was no clear desorption peak of N_2O during the TPD process, therefore, only NO and NO_2 contributed to the signal of m/z = 30 (I_{30}). By ignoring the mass discrimination factor, the

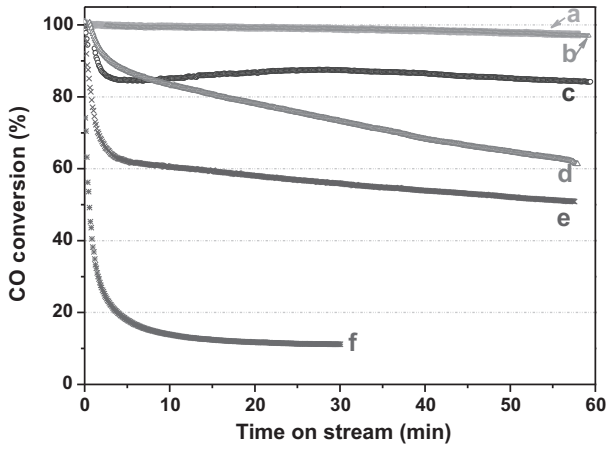

Fig. 5. CO conversion at GHSV = 60,000 h^{-1} over fresh Au/TiO_2 catalyst in the absence of any nitrogen oxides (a), and in the presence of 100 ppm of N_2O (b), NO (c) and NO_2 (d), and over the catalyst pre-adsorbed by 100 ppm NO_2 in N_2 for 30 min (e) and treated by 10% N_2/90% O_2 plasma (f).

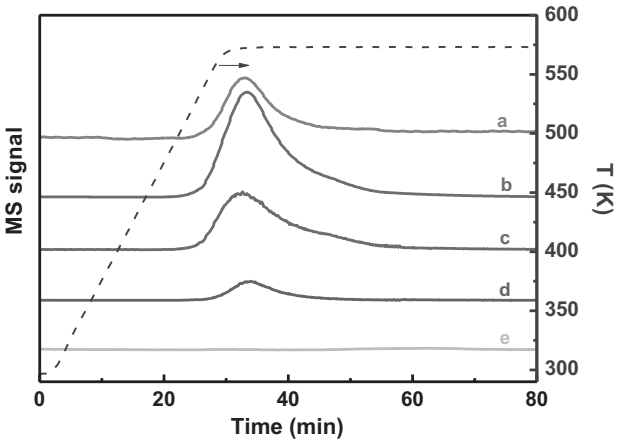

Fig. 6. TPD profiles of Au/TiO_2 catalyst treated in 10% N_2/90% O_2 plasma at (a) m/z = 32 (O_2), (b) m/z = 30 (NO + NO_2), (c) m/z = 30 (NO), (d) m/z = 46 (NO_2) and (e) m/z = 44 (N_2O).

contribution of NO to m/z = 30 (I_{NO}, Fig. 6c) was obtained by subtracting the contribution of NO_2 to m/z = 30 per the following equation:

$$I_{NO} = I_{30} - I_{46}\,\frac{\beta_{30}^{NO_2}}{\beta_{46}^{NO_2}} \qquad (R7)$$

where, $\beta_{46}^{NO_2}$ and $\beta_{30}^{NO_2}$ are the ratios of the partial ionization cross section of the respective ion fragment at m/z = 46 and 30 generated by NO_2 molecule to the total ionization cross section of NO_2 at 70 eV. According to the mass spectrometer manual, $\beta_{46}^{NO_2}$ is at 0.219 and $\beta_{30}^{NO_2}$ is at 0.591, at 70 eV.

Fig. 6 provided strong evidence for the formation of surface poisoning species (denoted as $[NO_y]_s$) on the Au/TiO_2 catalyst derived from N_2/O_2 plasma, which decomposed to release NO, NO_2 and O_2 after heating at 573 K.

Fig. 7 shows the UV–vis spectra of TiO_2 support, fresh Au/TiO_2 catalyst, Au/TiO_2 catalysts treated in 10% N_2/90% O_2 plasma, and the plasma-treated sample after TPD experiment. The absorption bands at 200–350 nm are ascribed to the TiO_2 support [35], while the absorption band at around 560 nm is attributed to metallic gold (Au^0) particle [36]. After N_2/O_2 plasma treatment, the adsorption peak of Au^0 species became flattened. This behavior was probably caused by the formation of surface poison species $[NO_y]_s$, which may change the surrounding chemical environment of the gold particles. The adsorption peak of Au^0 species after TPD was back

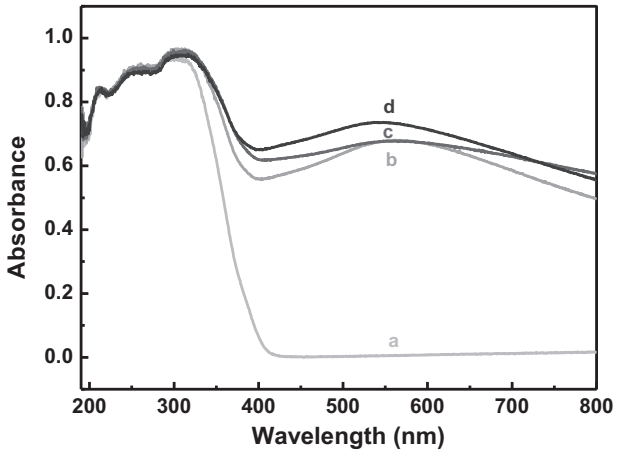

Fig. 7. UV–vis spectra of (a) TiO_2; (b) fresh Au/TiO_2; (c) Au/TiO_2 treated in 10% N_2/90% O_2 plasma; and (d) sample of (c) followed by TPD experiment.

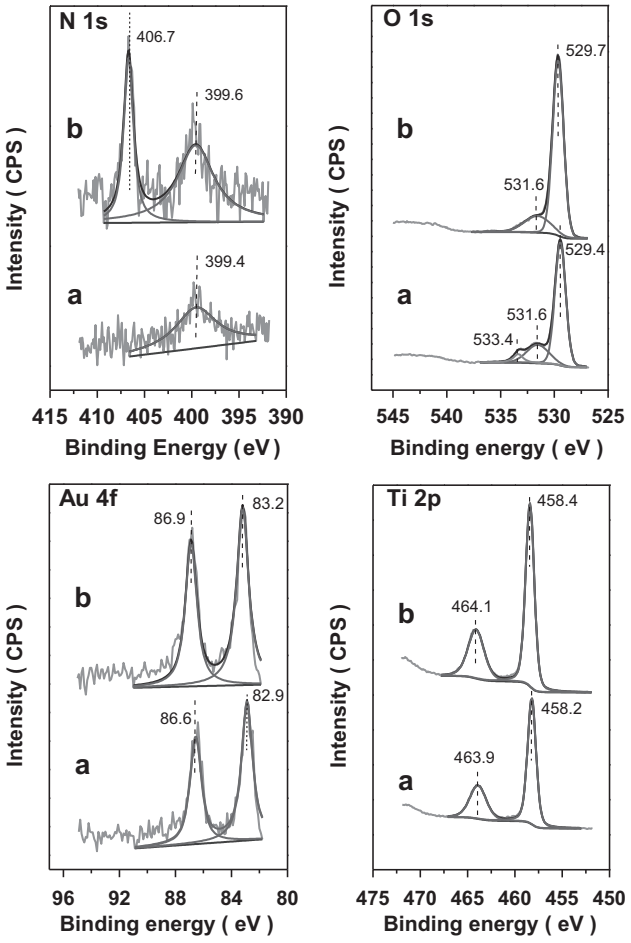

Fig. 8. XPS spectra of N 1s, O 1s, Au 4f and Ti 2p of (a) fresh Au/TiO_2 catalyst and (b) Au/TiO_2 catalyst treated in 10% N_2/90% O_2 plasma.

to initial status due to the decomposition and removal of $[NO_y]_s$. Accordingly, its catalytic activity was completely recovered.

To determinate changes in chemical environment of the Au/TiO_2 catalyst surface arisen from N_2/O_2 plasma treatment, high resolution XPS spectra of N 1s, O 1s, Au 4f and Ti 2p of fresh and plasma-treated samples were shown in Fig. 8. In the N 1 s spectrum of the plasma-treated sample, besides a weak peak at 399.6 eV (+0.2 eV shift vs. the fresh one) assigned to molecularly chemisorbed γ-N_2 [37], a new and strong peak at 406.7 eV was arisen from the $[NO_y]_s$. No signal peak was detected at ca. 396 eV, indicating that no nitriding of the titania surface occurred for the N_2/O_2 plasma-treated catalysts [37]. In the O 1s spectrum of the fresh sample, three individual peaks were resolved and attributed to oxygen from Ti—O bond at 529.4 eV, surface OH groups at 531.6 eV, and adsorbed H_2O at 533.4 eV [38], respectively. For the plasma-treated sample, the O 1s peak at 529.7 eV should be assigned to oxygen from TiO_2 and the $[NO_y]_s$. The Au 4f and Ti 2p peaks of the plasma-treated sample shifted to higher binding energy by 0.2–0.3 eV in comparison to the fresh sample. This shift reflected that the chemical states of Au, Ti and O were affected by the nature of the $[NO_y]_s$ on the plasma-treated catalyst.

The formation of surface poisoning species $[NO_y]_s$ was also verified by DRIFT spectra. Fig. 9 exhibits the DRIFT spectra of the fresh catalyst, the catalyst treated in 10% N_2/90% O_2 plasma, and the catalyst treated in 10% N_2/90% O_2 plasma followed by TPD experiment. Upon N_2/O_2 plasma treatment, some new IR bands at 1603 cm^{-1}, 1584 cm^{-1}, 1302 cm^{-1}, a shoulder at 1261 cm^{-1} and a broad band around 1437 cm^{-1} appeared. However, all of the bands disappeared after TPD, which suggested that the surface poisoning species $[NO_y]_s$ have been removed completely. To distinguish poisoning species $[NO_y]_s$ from nitrate species, the DRIFT spectrum of the Au/TiO_2 catalyst after NO_2 adsorption was also measured. As shown in Fig. 9d, IR bands at 1614 cm^{-1} and 1252 cm^{-1} are assigned

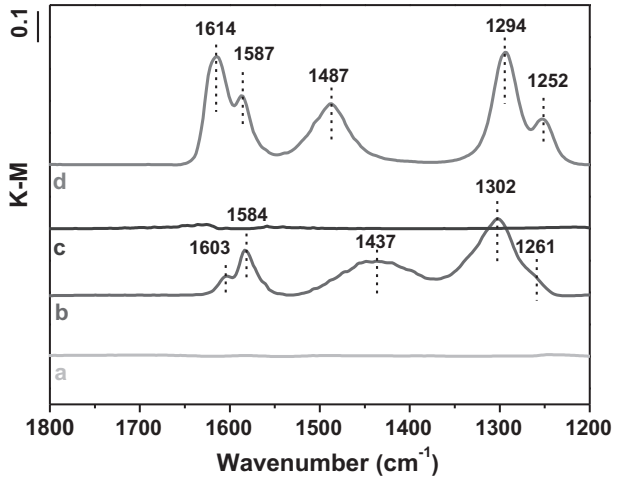

Fig. 9. DRIFT spectra of (a) fresh Au/TiO_2 catalyst; (b) Au/TiO_2 catalyst treated in 10% N_2/90% O_2 plasma; (c) sample (b) followed by TPD experiment; and (d) Au/TiO_2 catalyst after NO_2 adsorption (200 ppm NO_2 in N_2, 100 ml/min for 120 min).

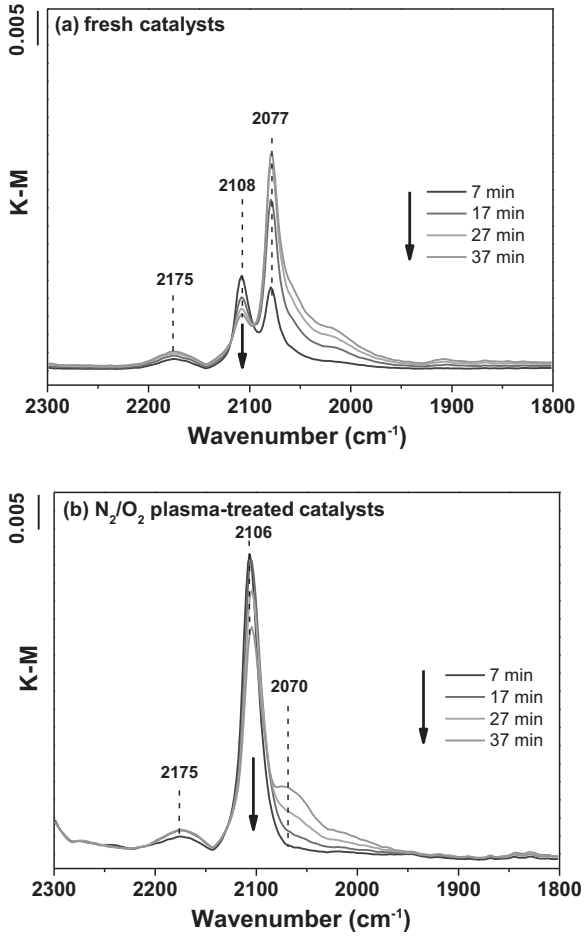

Fig. 10. DRIFT spectra of CO adsorption (1% CO in He, 100 mL/min) after 7, 17, 27 and 37-min exposure at room temperature on (a) fresh Au/TiO_2 catalyst; and (b) Au/TiO_2 catalyst treated by 10% N_2/90% O_2 plasma.

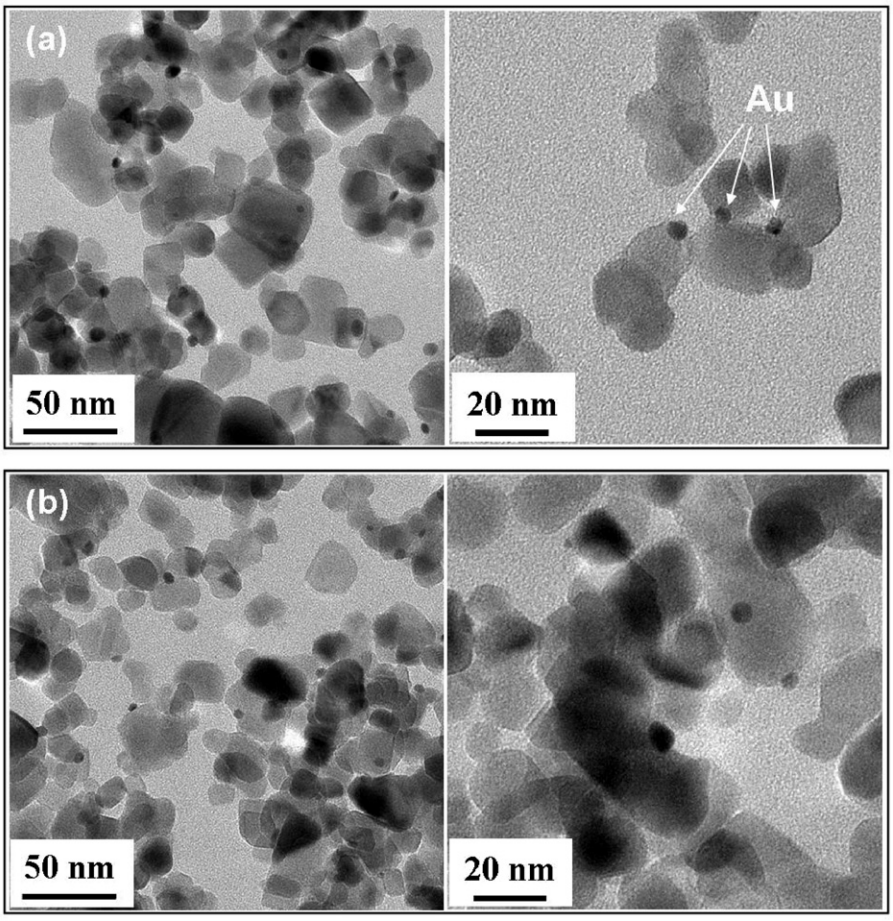

Fig. 11. TEM images of (a) fresh Au/TiO_2 catalyst; and (b) Au/TiO_2 catalyst treated in 10% N_2/90% O_2 plasma.

to bridged nitrate species, the bands at 1294 cm^{-1} and 1487 cm^{-1} are attributed to monodentate nitrate species, and the band at 1587 cm^{-1} is probably ascribed to the presence of bidentate nitrate species [39,40]. Obviously, the spectrum after NO_2 adsorption was different from that after N_2/O_2 plasma treatment. It was deemed that the formation of surface poisoning species $[NO_y]_s$ could be attributed to N_2O_5 adsorption. However, due to the instability of N_2O_5 molecule, it was rarely used as a probe molecule in the literature for IR study, and in this work, we did not attempt to use it either to evaluate its direct contribution to the formation of surface poisoning species $[NO_y]_s$.

Fig. 10 plots the DRIFT spectra of CO adsorption on the fresh catalyst and the catalyst treated in 10% N_2/90% O_2 plasma at various exposure times at room temperature. For the fresh catalyst, as shown in Fig. 10a, two sharp bands was observed at 2108 cm^{-1} and 2077 cm^{-1} and they are ascribed to linearly adsorbed CO on Au^0 [41,42] and TiO_2 support [42], respectively. With increasing exposure time, the band at 2077 cm^{-1} intensified along with a reduction in intensity of the band at 2108 cm^{-1}. For the plasma-treated catalyst, as shown in Fig. 10b, a strong and sharp band at 2106 cm^{-1} appeared, indicating that Au^0–CO interaction became stronger on the plasma-treated catalyst. With increasing exposure time, the intensity of the band at 2106 cm^{-1} slowly decreased, accompanied with slow protruding of a shoulder at around 2070 cm^{-1}. This may be referred to the reduction of the $[NO_y]_s$ on the plasma-treated catalysts by carbon monoxide. Therefore, the poisoning effect of the $[NO_y]_s$ on the plasma-treated catalysts is very likely attributed to the $[NO_y]_s$ occupying surface anion vacancies of TiO_2 support and blocking adsorption of oxygen molecules. The weak and broad band at 2175 cm^{-1} on both fresh and plasma-treated catalysts, is assigned to the adsorption of CO on either the support or Au^{n+} [43].

3.3.3. TEM observations

Since the catalyst particle size or morphology may affect catalyst activity, it would be worthwhile to identify any changes in particle size or morphology of the Au/TiO_2 catalyst after plasma regeneration. Fig. 11 shows TEM images of fresh Au/TiO_2 catalyst and the catalyst treated in 10% N_2/90% O_2 plasma. The gold particle size did not change clearly before and after plasma treatment. The gold particles were mostly spherical shape with about 5 nm in diameter. No obvious aggregation of the gold particles was observed after plasma treatment. Therefore, the catalyst activity loss owing to any particle size change of gold upon plasma treatment can be excluded. It further suggested that the catalyst poisoning in N_2/O_2 plasma should be related to the surface poisoning species $[NO_y]_s$.

4. Conclusions

For the first time, in-situ regeneration of deactivated Au/TiO_2 catalyst during CO oxidation was investigated by N_2/O_2 plasma. Interestingly, pure O_2 plasma could reversibly regenerate the deactivated Au/TiO_2 catalyst during CO oxidation. However, the existence of N_2 in the plasma caused an extra poisoning effect on catalyst. The poisoning effect was the most severe at 10% N_2, and became much weaker at 80% N_2. This trend was well correlated to the N_2O_5 concentration in gaseous products of N_2/O_2 plasma, as detected by on-line FT-IR.

The poisoning effect was further studied by various techniques, and it was proposed that it was related to the formation of surface poisoning species $[NO_y]_s$ on Au/TiO_2 catalyst during N_2/O_2 plasma regeneration. The $[NO_y]_s$ on Au/TiO_2 catalyst resulted in a flattened UV–vis adsorption peak of Au^0 species and a shift to higher XPS binding energy of Au 4f and Ti 2p. DRIFT spectra revealed that the surface poisoning species $[NO_y]_s$ were different from the species formed upon NO_2 adsorption. The surface poisoning species $[NO_y]_s$ could be removed by heat treatment at 573 K to fully restore the catalyst activity. DRIFT investigation of CO adsorption implied that the $[NO_y]_s$ species may occupy surface anion vacancies of TiO_2 support, block adsorption of oxygen molecules and lead to catalyst poisoning. No change in gold particle size was observed by TEM before and after N_2/O_2 plasma regeneration, which further suggested that the surface poisoning species $[NO_y]_s$ formed on Au/TiO_2 catalysts accounted for the catalyst poisoning during N_2/O_2 plasma regeneration.

Acknowledgements

This work is supported by National Natural Science Foundation of China (11175036, 11079013).

References

[1] M. Haruta, T. Kobayashi, H. Sano, N. Yamada, Chem. Lett. 16 (1987) 405–408.
[2] C.H. Christensen, J.K. Norskov, Science 327 (2010) 278–279.
[3] T. Davran-Candan, S.T. Tezcanli, R. Yildirim, Catal. Commun. 12 (2011) 1149–1152.
[4] L.C. Wang, Q. Liu, X.S. Huang, Y.M. Liu, Y. Cao, K.N. Fan, Appl. Catal. B: Environ. 88 (2009) 204–212.
[5] M. Kipnis, E. Volnina, Appl. Catal. B: Environ. 103 (2011) 39–47.
[6] V. Rodriguez-Gonzalez, R. Zanella, L.A. Calzada, R. Gomez, J. Phys. Chem. C 113 (2009) 8911–8917.
[7] X.H. Zou, S.X. Qi, ZhH. Suo, L.D. An, F. Li, Catal. Commun. 8 (2007) 784–788.
[8] P. Konova, A. Naydenov, C. Venkov, D. Mehandjiev, D. Andreeva, T. Tabakova, J. Mol. Catal. A: Chem. 213 (2004) 235–240.
[9] T.V. Choudhary, D.W. Goodman, Top. Catal. 21 (2002) 25–34.
[10] H.S. Oh, C.K. Costello, C. Cheung, H.H. Kung, M.C. Kung, Stud. Surf. Sci. Catal. 139 (2001) 375–381.
[11] R. Zanella, C. Louis, Catal. Today 107–108 (2005) 768–777.
[12] H.S. Oh, J.H. Yang, C.K. Costello, Y.M. Wang, S.R. Bare, H.H. Kung, M.C. Kung, J. Catal. 210 (2002) 375–386.
[13] M. Raphulu, J. McPherson, G. Pattrick, T. Ntho, L. Mokoena, J. Moma, E. van der Lingen, Gold Bull. 42 (2009) 328–336.
[14] T.A. Ntho, J.A. Anderson, M.S. Scurrell, J. Catal. 261 (2009) 94–100.
[15] C.H. Tseng, T. Yang, H.E. Wu, H.C. Chiang, J. Hazard. Mater. 166 (2009) 686–694.
[16] Y. Hao, M. Mihaylov, E. Ivanova, K. Hadjiivanov, H. Knozinger, B.C. Gates, J. Catal. 261 (2009) 137–149.
[17] T. Diemant, J. Bansmann, R.J. Behm, Vacuum 84 (2009) 193–196.
[18] H.H. Kung, M.C. Kung, C.K. Costello, J. Catal. 216 (2003) 425–432.
[19] C.K. Costello, M.C. Kung, H.S. Oh, Y. Wang, H.H. Kung, Appl. Catal. A: Gen. 232 (2002) 159–168.
[20] J. Van Durme, J. Dewulf, C. Leys, H. Van Langenhove, Appl. Catal. B: Environ. 78 (2008) 324–333.
[21] Z.H. Wei, C.J. Liu, Mater. Lett. 65 (2011) 353–355.
[22] H. Furusho, K. Kitano, S. Hamaguchi, Y. Nagasaki, Chem. Mater. 21 (2009) 3526–3535.
[23] R. Sharma, R.D. Rimmer, J. Gunamgari, R.S. Shekhawat, B.J. Davis, M.K. Mazumder, D.A. Lindquist, IEEE Trans. Ind. Appl. 41 (2005) 1373–1376.
[24] H.H. Kim, S. Tsubota, M. Date, A. Ogata, S. Futamura, Appl. Catal. A: Gen. 329 (2007) 93–98.
[25] W.B. DeMore, S.P. Sander, D.M. Golden, R.F. Hampson, M.J. Kurylo, C.J. Howard, A.R. Ravishankara, C.E. Kolb, M.J. Molina, JPL Publication 97-4 (1997) 1–266.
[26] M. Gonzalez, I. Miquel, R. Sayos, Chem. Phys. Lett. 335 (2001) 339–347.
[27] M.F. Golde, Int. J. Chem. Kinet. 20 (1988) 75–92.
[28] Q. Sun, A.M. Zhu, X.F. Yang, J.H. Niu, Y. Xu, Chem. Commun. (2003) 1418–1419.
[29] R. Atkinson, D.L. Baulch, R.A. Cox, R.F. Hampson, J.A. Kerr, M.J. Rossi, J. Troe, J. Phys. Chem. Ref. Data 26 (1997) 1329–1499.
[30] J.T. Herron, Plasma Chem. Plasma Process. 21 (2001) 581–609.
[31] A.M. Zhu, Q. Sun, J.H. Niu, Y. Xu, Z.M. Song, Plasma Chem. Plasma Process. 25 (2005) 371–386.
[32] W. Tsang, J.T. Herron, J. Phys. Chem. Ref. Data 20 (1991) 609–663.
[33] R. Atkinson, D.L. Baulch, R.A. Cox, R.F. Hampson, J.A. Kerr, J. Troe, J. Phys. Chem. Ref. Data 21 (1992) 1125–1568.
[34] J.T. Herron, D.S. Green, Plasma Chem. Plasma Process. 21 (2001) 459–481.
[35] R. Zanella, S. Giorgio, C.H. Shin, C.R. Henry, C. Louis, J. Catal. 222 (2004) 357–367.
[36] J. Huang, W.L. Dai, H.X. Li, K. Fan, J. Catal. 252 (2007) 69–76.
[37] C. Chen, H. Bai, C. Chang, J. Phys. Chem. C 111 (2007) 15228–15235.
[38] J. Pouilleau, D. Devilliers, F. Garrido, S. Durand-Vidal, E. Mahé, Mater. Sci. Eng. B 47 (1997) 235–243.
[39] M.A. Debeila, N.J. Coville, M.S. Scurrell, G.R. Hearne, Appl. Catal. A: Gen. 291 (2005) 98–115.
[40] M.A. Debeila, N.J. Coville, M.S. Scurrell, G.R. Hearne, M.J. Witcomb, J. Phys. Chem. B 108 (2004) 18254–18260.
[41] M.A. Debeila, N.J. Coville, M.S. Scurrell, G.R. Hearne, Catal. Today 72 (2002) 79–87.
[42] M.A. Bollinger, M.A. Vannice, Appl. Catal. B: Environ. 8 (1996) 417–443.
[43] M.C. Raphulu, J. McPherson, E. van der Lingen, J.A. Anderson, M.S. Scurrell, Gold Bull. 43 (2010) 334–344.